Distributed sensing: multiple capacitive stretch sensors on a single channel

Andreas Tairych[a] and Iain A. Anderson[a,b,c]

[a]Biomimetics Lab, Auckland Bioengineering Institute, University of Auckland, 70 Symonds Street, Auckland, New Zealand
[b]Engineering Science, University of Auckland, 70 Symonds Street, Auckland, New Zealand
[c]StretchSense Ltd, 114 Rockfield Road, Auckland, New Zealand

ABSTRACT

"Soft, stretchable, and unobtrusive". These are some of the attributes frequently associated with capacitive dielectric elastomer (DE) sensors for body motion capture. While the sensors themselves are soft and elastic, they require rigid peripheral components for capacitance measurement. Each sensor is connected to a separate channel on the sensing circuitry through its own set of wires. In wearable applications with large numbers of sensors, this can lead to a considerable circuit board footprint, and cumbersome wiring. The additional equipment can obstruct movement and alter user behaviour.

Previous work has demonstrated how a transmission line model can be applied to localise deformation on a single DE sensor. Building on this approach, we have developed a distributed sensing method by arranging capacitive DE sensors and external resistors to form a transmission line, which is connected to a single sensing channel with only one set of wires. The sensors are made from conductive fabric electrodes, and silicone dielectrics, and the external resistors are off-the-shelf metal film resistors. Excitation voltages with different frequencies are applied to the transmission line. The lumped transmission line capacitances at these frequencies are passed on to a mathematical model that calculates individual sensor capacitance changes. The prototype developed for this study is capable of obtaining separate readings for simultaneously stretched sensors.

Keywords: Distributed Sensing, Transmission Line, Conductive Fabric Sensors, Dielectric Elastomer Sensors, Wearable Sensors, Body Motion Sensing

1. INTRODUCTION

Sports training, physiotherapy, the entertainment industry, and human-machine interaction provide various opportunities for body motion sensing. Examples include the recording of athletes' or patients' movements, capturing an actor's motion to provide motion data for computer-generated imagery, or designing wearable and immersive user interfaces for computers. Capacitive dielectric elastomer (DE) sensors are well suited for such applications, because they are soft, compliant, and easy to integrate into sensing garments. To retain the advantages of these sensors, wiring and circuit board footprint should be kept to a minimum.

Researchers have explored the arrangement of capacitive sensors in arrays as a means to reducing wiring complexity. Conductive polymers,[1–3] and conductive fabric or fibres[4–6] are commonly used electrode materials. An array can either be made from individual conductive patches sharing a common electrode,[5] or from perpendicular electrode strips.[4,6] Capacitances between overlapping areas are not measured simultaneously, but sequentially, using time-division multiplexing. Each row and column requires an electrical connection, thus an increase of array size results in a proportionate number of wires.

Further author information: (Send correspondence to A.T.)
A.T.: E-mail: atai732@aucklanduni.ac.nz

Electroactive Polymer Actuators and Devices (EAPAD) 2017, edited by Yoseph Bar-Cohen, Proc. of SPIE
Vol. 10163, 1016306 · © 2017 SPIE · CCC code: 0277-786X/17/$18 · doi: 10.1117/12.2260416

Xu et al. presented a multi-frequency method that avoids this disadvantage.[7–9] Instead of assembling an array from separate capacitive DE sensors, a single continuous sensor was approximated by a series of n R-C elements, i.e. an R-C transmission line. Each element represented a section of the sensor area. Sinusoidal excitation signals with n different frequencies were applied simultaneously. Signals at higher frequencies were attenuated more than those at lower frequencies, and therefore less charge was transferred to transmission line nodes further down the sensor strip. Consequently, deforming one of these sensor areas resulted in a lower measured capacitance change at higher excitation frequencies. Capacitance changes occurring at different frequencies were processed by an algorithm to determine the part of the sensor that was deformed. Two-dimensional location sensing was achieved using two sensors that were bonded together. This method only requires two sensors with two pairs of electrical connections.

The distributed sensing method described in the following sections shares the multi-frequency transmission line approach. But in the place of one continuous sensor we use multiple discrete sensors connected together along a single transmission line. This enables the economic deployment of arrays of discrete sensors that are coupled to a single set of electronics.

2. FABRIC SENSOR TRANSMISSION LINE

A transmission line assembled from conductive fabric sensors and external resistors, is the basis of the distributed sensing method. Conductive fabric is made from silver- or stainless steel fibres, embedded in a non conductive fabric substrate, and has therefore low resistance. The fabric electrodes are separated by layers of silicone dielectrics, as illustrated in Fig. 1. The outer electrodes are electrically connected, which provides shielding, and thus avoids capacitance changes due to proximity.

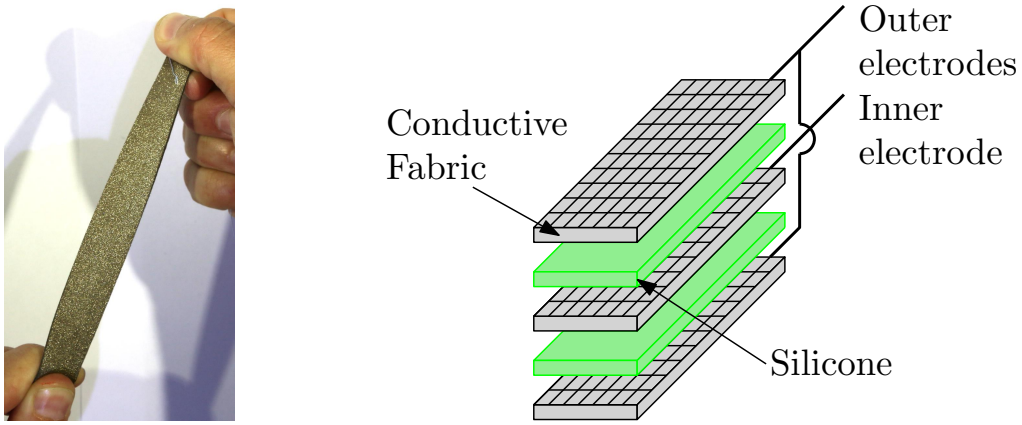

Figure 1. Capacitive conductive fabric strain sensors

When the sensor is stretched, its area increases, and the thickness of the dielectrics decreases, which causes capacitance to increase, as described in Eq. 1 where ϵ_0 is vacuum permittivity, ϵ_r is the relative permittivity of the silicone dielectric, A represents the electrode area, and t is the thickness of the dielectric:

$$C = 2 \cdot \frac{\epsilon_0 \cdot \epsilon_r \cdot A}{t} \tag{1}$$

Fig. 2 shows a circuit diagram of the transmission line with three sensors. The leakage current across the dielectric is neglected because of the low excitation voltage amplitudes. Hence, there are no leakage resistors in parallel to the capacitors. No series resistors were added to the capacitors to model electrode resistance, because of the relatively low resistance of conductive fabric. Inductance is estimated as 1 μH for a metre of wire. When compared to capacitive reactance, inductive reactance is negligible on the basis of this estimation.

V_E refers to the sum of the simultaneously applied excitation signals, with f_1 being the lowest, and f_3 being the highest frequency. V_{R3} is proportional to the current I. With R_3 integrated into the sensing circuit, the transmission line is connected to the sensing circuitry with only two wires.

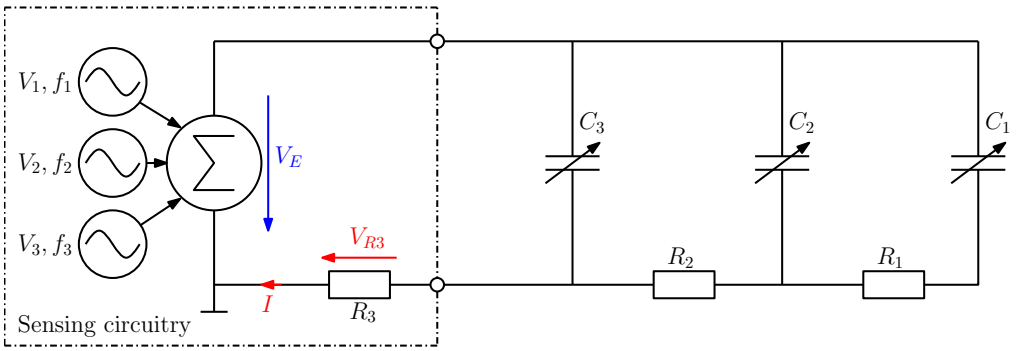

Figure 2. Schematic of the R-C transmission line with three sensors

Individual capacitance changes are established based on the total capacitance of the transmission line at each frequency. This is a lumped capacitance that is calculated from the voltages V_E, V_{R3}, and the known value of R_3, according to the geometric relationship shown in Fig. 3. An FFT, performed on V_E and V_{R3}, yields the amplitudes and phase shift between these two voltages at each frequency. Impedance, and furthermore reactance are calculated from these parameters. Finally, three lumped transmission line capacitances at f_1, f_2 and f_3 are determined from reactances and frequencies.

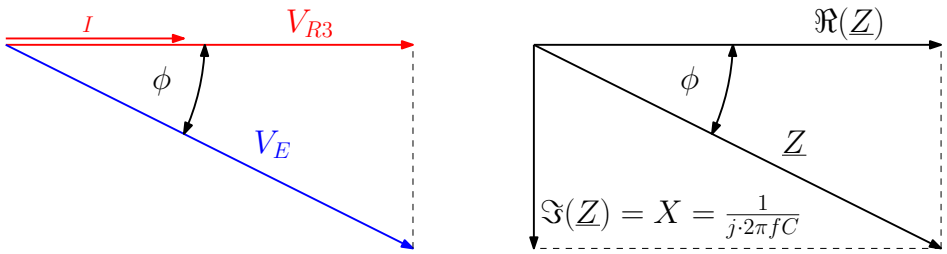

Figure 3. Vector diagrams of measured voltages and transmission line impedance

Modelling the transmission line capacitance as a lumped parameter results in decreasing capacitance values as the frequency increases. While all three capacitors are charged equally at a sufficiently low frequency, the effect of signal attenuation caused by the external resistors becomes more pronounced at higher frequency. As a result, the lumped transmission line capacitance at high frequencies is lower than C_1, C_2 and C_3 in parallel.

The frequency sweep shown in Fig. 4 illustrates this effect. The black line represents the resting capacitance of the transmission line, where all sensors remain in the relaxed position. The coloured lines represent the transmission line capacitance with individually stretched sensors. At 1 kHz, stretching sensor 1 leads to an increase of transmission line capacitance of approximately 90 pF. This capacitance change decreases with increasing frequency, until it entirely disappears in the vicinity of 11 kHz. This indicates that there is no difference between sensor 1 being stretched or relaxed at 11 kHz.

A similar effect can be observed for sensor 2. The frequency change caused by stretching sensor 3, on the other hand, contributes to the lumped transmission line capacitance C throughout the entire examined frequency range.

This frequency dependence of transmission line capacitance is subsequently utilised to calculate individual sensor capacitance changes.

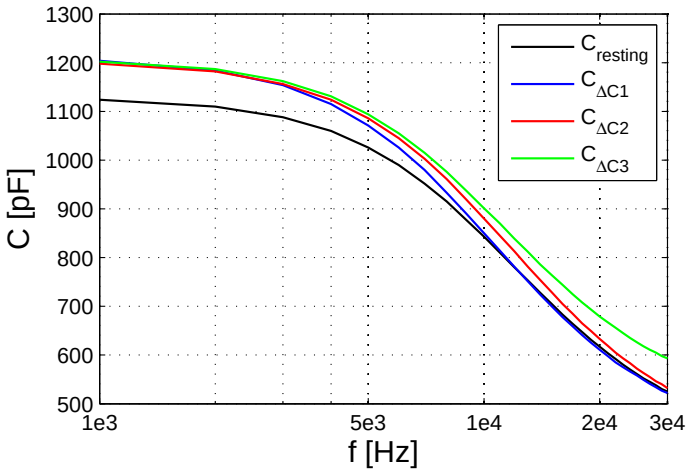

Figure 4. Frequency sweep of transmission line capacitances with sensors in the relaxed position, and stretched individually by 30 mm; $C_{\Delta C1}$ is the transmission line capacitance with sensor 1 being stretched.

3. MATHEMATICAL MODEL

Fig. 5 is a symbolic representation of the transmission line capacitance at frequencies f_1, f_2 and f_3. At each frequency, the overall capacitances C_{f1}, C_{f2} and C_{f3} are the sums of the respective resting capacitance, and the capacitance change of each sensor. $\Delta C_{fj,Ci}$ are capacitance changes at frequency f_j, caused by sensor capacitance C_i. Subsequently, the index j is used to designate the frequency number, and the index i refers to the sensor number.

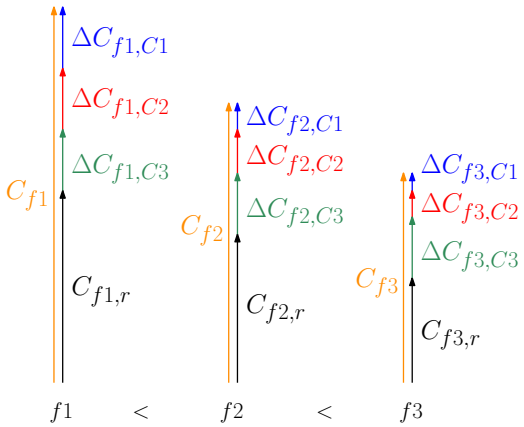

Figure 5. Representation of transmission line capacitance at f_1, f_2 and f_3

The relationship illustrated in Fig. 5 is expressed mathematically in Eq. 2. The goal is to obtain the capacitance changes $\Delta C_{fj,Ci}$.

$$\begin{aligned} C_{f1} &= C_{f1,r} + \Delta C_{f1,C1} + \Delta C_{f1,C2} + \Delta C_{f1,C3} \\ C_{f2} &= C_{f2,r} + \Delta C_{f2,C1} + \Delta C_{f2,C2} + \Delta C_{f2,C3} \\ C_{f3} &= C_{f3,r} + \Delta C_{f3,C1} + \Delta C_{f3,C2} + \Delta C_{f3,C3} \end{aligned} \tag{2}$$

To solve this system of equations for $\Delta C_{fj,Ci}$, six of the nine capacitance changes must be eliminated. This can be achieved by expressing capacitance changes at frequencies f_2 and f_3 as fractions of capacitance changes at frequency f_1. The factors for establishing this linear relationship are calculated based on the sketch in Fig. 6. $C_{f1,r}$ and $C_{f2,r}$ are the transmission line resting capacitances. $C_{f1,C1}$ and $C_{f2,C1}$ are the transmission line capacitances when sensor 1 is being stretched, and sensor 2 and 3 remain in the relaxed position.

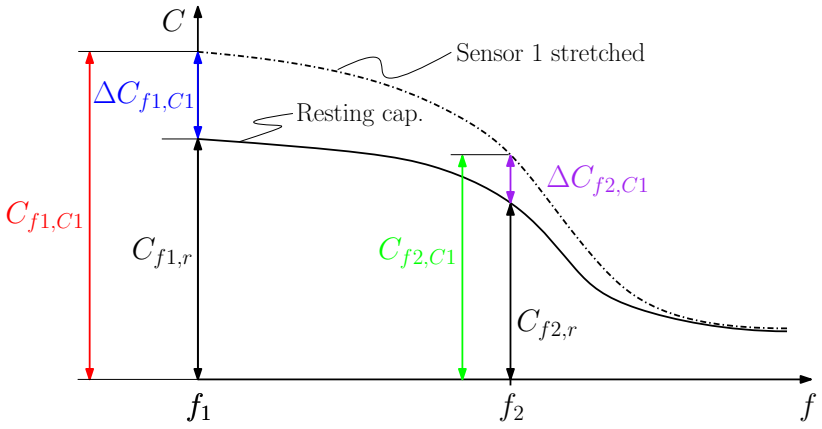

Figure 6. Resting capacitances and capacitance changes at f_1 and f_2

The relationship between the capacitance changes at frequencies f_1 and f_2 is expressed in Eq. 3.

$$\Delta C_{f2,C1} = \Delta C_{f1,C1} \cdot \frac{C_{f2,C1} - C_{f2,r}}{C_{f1,C1} - C_{f1,r}} \tag{3}$$

Repeating this procedure for the remaining capacitance changes at f_2 and f_3 yields:

$$\begin{aligned}
C_{f1} &= C_{f1,r} + \Delta C_{f1,C1} + \Delta C_{f1,C2} + \Delta C_{f1,C3} \\
C_{f2} &= C_{f2,r} + \Delta C_{f1,C1} \cdot \frac{C_{f2,C1} - C_{f2,r}}{C_{f1,C1} - C_{f1,r}} + \Delta C_{f1,C2} \cdot \frac{C_{f2,C2} - C_{f2,r}}{C_{f1,C2} - C_{f1,r}} + \Delta C_{f1,C3} \cdot \frac{C_{f2,C3} - C_{f2,r}}{C_{f1,C3} - C_{f1,r}} \\
C_{f3} &= C_{f3,r} + \Delta C_{f1,C1} \cdot \frac{C_{f3,C1} - C_{f3,r}}{C_{f1,C1} - C_{f1,r}} + \Delta C_{f1,C2} \cdot \frac{C_{f3,C2} - C_{f3,r}}{C_{f1,C2} - C_{f1,r}} + \Delta C_{f1,C3} \cdot \frac{C_{f3,C3} - C_{f3,r}}{C_{f1,C3} - C_{f1,r}}
\end{aligned} \tag{4}$$

Substituting coefficients a_{ij} for the fractions in Eq. 4 yields Eq. 5.

$$\begin{aligned}
C_{f1} - C_{f1,r} &= \Delta C_{f1,C1} + \Delta C_{f1,C2} + \Delta C_{f1,C3} \\
C_{f2} - C_{f2,r} &= \Delta C_{f1,C1} \cdot a_{12} + \Delta C_{f1,C2} \cdot a_{22} + \Delta C_{f1,C3} \cdot a_{13} \\
C_{f3} - C_{f3,r} &= \Delta C_{f1,C1} \cdot a_{13} + \Delta C_{f1,C2} \cdot a_{23} + \Delta C_{f1,C3} \cdot a_{33}
\end{aligned} \tag{5}$$

Coefficients a_{ij} and resting capacitances $C_{fj,r}$ are determined in one-off measurements, and remain therefore constant in the implementation of the distributed sensing algorithm. In contrast, capacitances C_{fj} are measured continuously. The system of equations can now be solved for capacitance changes $\Delta C_{f1,Ci}$. Because the frequency index f_1 is common to all capacitance changes, it can be omitted. Hence, ΔC_i in Eq. 5 are substituted for $\Delta C_{f1,Ci}$. The factors α in Eq. 6 result from solving Eq. 5, and consist of coefficients a_{ij}. By implementing Eq. 6 in LabVIEW, separate capacitance changes for each sensor can be acquired in real time, from constant parameters and continuous measurements.

$$\begin{aligned}
\Delta C_1 &= (C_{f1} - C_{f1,r}) \cdot \alpha_{11} + (C_{f2} - C_{f2,r}) \cdot \alpha_{21} + (C_{f3} - C_{f3,r}) \cdot \alpha_{31} \\
\Delta C_2 &= (C_{f1} - C_{f1,r}) \cdot \alpha_{12} + (C_{f2} - C_{f2,r}) \cdot \alpha_{22} + (C_{f3} - C_{f3,r}) \cdot \alpha_{32} \\
\Delta C_3 &= (C_{f1} - C_{f1,r}) \cdot \alpha_{13} + (C_{f2} - C_{f2,r}) \cdot \alpha_{23} + (C_{f3} - C_{f3,r}) \cdot \alpha_{33}
\end{aligned} \tag{6}$$

4. EXPERIMENT SETUP

The main components of the prototype can be seen in the block diagram in Fig. 7. All algorithms for signal generation, data acquisition, FFT, as well as Eq. 6 are implemented in LabVIEW. A Digilent Analog Discovery signal generation and data acquisition device interfaces LabVIEW with the hardware. It generates three sinusoidal excitation voltages, and measures the current-proportional voltage V_{R3} and the excitation voltage V_E. A custom built circuit passes the outgoing and incoming signals through voltage followers for decoupling.

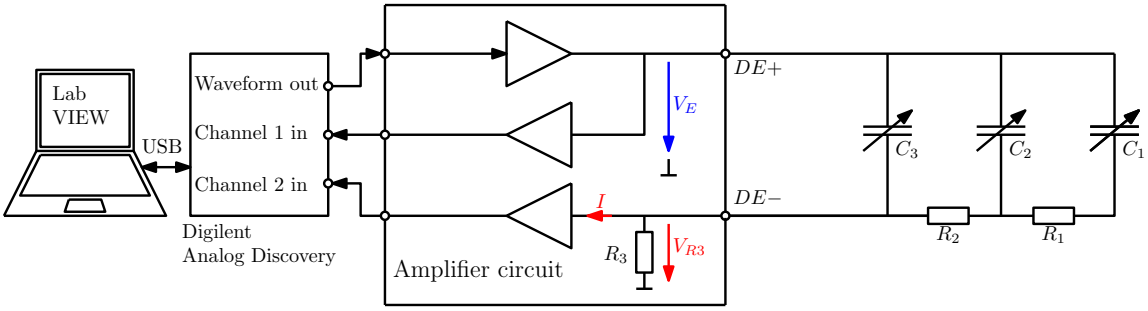

Figure 7. Block diagram of the distributed sensing system with three sensors

Fig. 8 shows a picture of the prototype. The sensors have a length of 120 mm, and a width of 19 mm when they are relaxed. Each sensor is attached to an acrylic glass frame, with a pre-strain of approximately 5 mm. The frames have hole patterns with a pitch of 10 mm to allow defined elongations. The electrodes are connected to a short coaxial cable with a female two-pin connector on the end. The external resistors R_1 and R_2 are metal film resistors. The white (DE+) and green (DE-) connector on the amplifier box are connected to two wires leading to the transmission line. The sensors are also interconnected with only two wires.

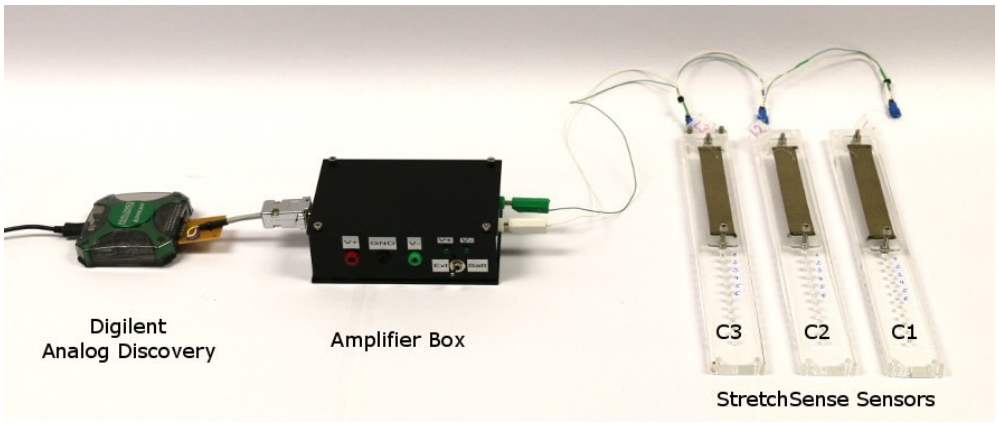

Figure 8. The prototype comprising signal generation and data acquisition device, amplifier box, and sensors

Resting capacitances of the prestrained sensors are C_1=450 pF, C_2=354 pF, and C_3=367 pF, when measured with a Hioki IM3523 LCR meter at 1 kHz. Resistances and capacitances define time constants, which in turn determine the sensing frequency range. Resistances in the range of tens of kΩ result in frequencies in the range of tens of kHz, which allow for relatively basic electronic circuit design. 21.5 kΩ were chosen for R_1 and R_2. R_3 has a resistance of 30 kΩ.

The lowest frequency f_1 was chosen to be 1 kHz. The frequency f_2 was 11 kHz, which is approximately where the capacitance change caused by sensor 1 disappears in the frequency sweep in Fig. 4. At f_3 = 21 kHz , the capacitance change caused by sensor 2 becomes very low. The amplitudes of the excitation voltages V_1, V_2 and V_3 are 3 V each.

5. RESULTS AND DISCUSSION

To experimentally determine the coefficients a_{ij}, every sensor was stretched step-wise and individually, with elongations ranging from the resting position to 60 mm. Every elongation was held constant for approximately 30 seconds. Recorded lumped transmission line capacitances are shown in Fig. 9. In accordance with the results of the frequency sweep in Fig. 4, stretching sensor 3 causes an increase of transmission line capacitance at all frequencies. When sensor 2 was stretched, there was almost no response at f_3. Finally, when sensor 1 was stretched, a capacitance change only occurred at the lowest frequency, f_1. The coefficients a_{ij} were calculated for each step in Fig. 9, which resulted in an array of six values for every coefficient. The resting position was an exception, because the coefficients are not mathematically defined for this case.

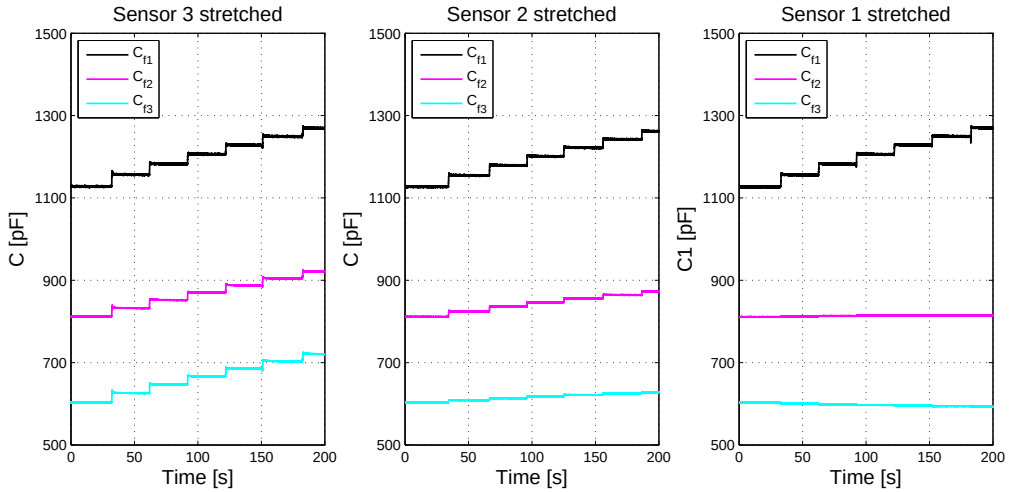

Figure 9. Changes of the lumped transmission line capacitance due to stepwise stretching

Fig. 10 shows plots of the coefficients a_{ij} over elongations ranging from 10 mm to 60 mm. The values varied with stretch, which indicated that the linear relationship between capacitance changes at different frequencies assumed in Eq. 3 is only an approximation of a nonlinear system. For the further implementation in LabVIEW, the average of each array of coefficients was used.

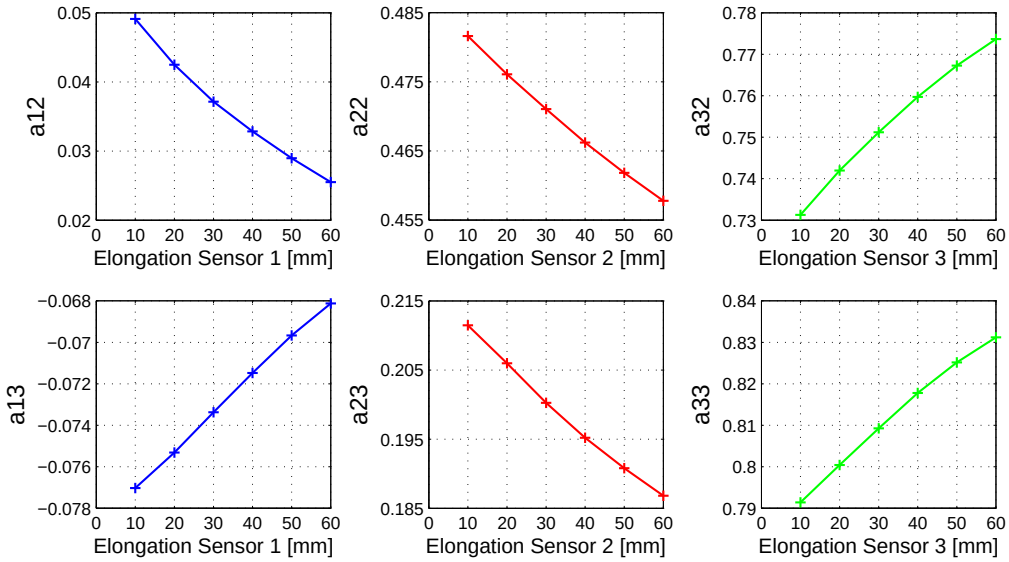

Figure 10. Values of dimensionless coefficients a_{ij} at different elongations

With the average coefficient values known, capacitance changes can be calculated in real time using Eq. 6. To investigate the relationship between capacitance change and strain, each sensor was stretched individually in 10 mm steps, beginning at the resting position, to a maximum elongation of 60 mm. Fig. 11 shows that capacitance increased as expected when a sensor was stretched. Reference measurements were carried out with a HIOKI IM3523 LCR meter. On average, a difference of 3% occurred between these results, and the ones obtained with the distributed sensing method. There is, however, also a response from the stationary sensors. This crosstalk was most likely a consequence of the coefficients a_{ij} varying with elongation. The largest crosstalk of approximately 7% occurred in sensor 2 on the right hand side plot in Fig. 11. Crosstalk changed its sign at 30 mm to 35 mm, possibly because of the averaging of coefficient values across the elongation range.

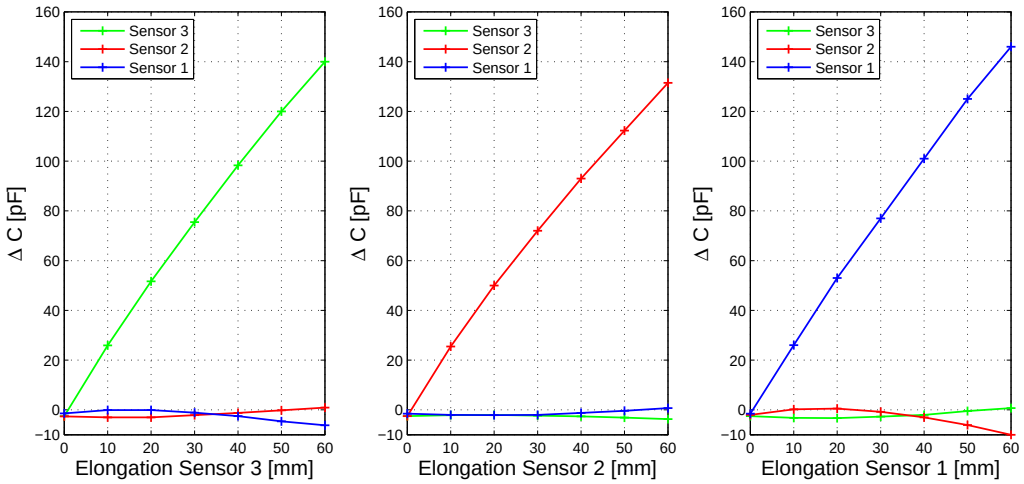

Figure 11. Capacitance changes due to individual stretch

In the last experiment, capacitance was recorded over time. The first half of the plot in Fig. 12 shows capacitance changes caused by individually stretched sensors.

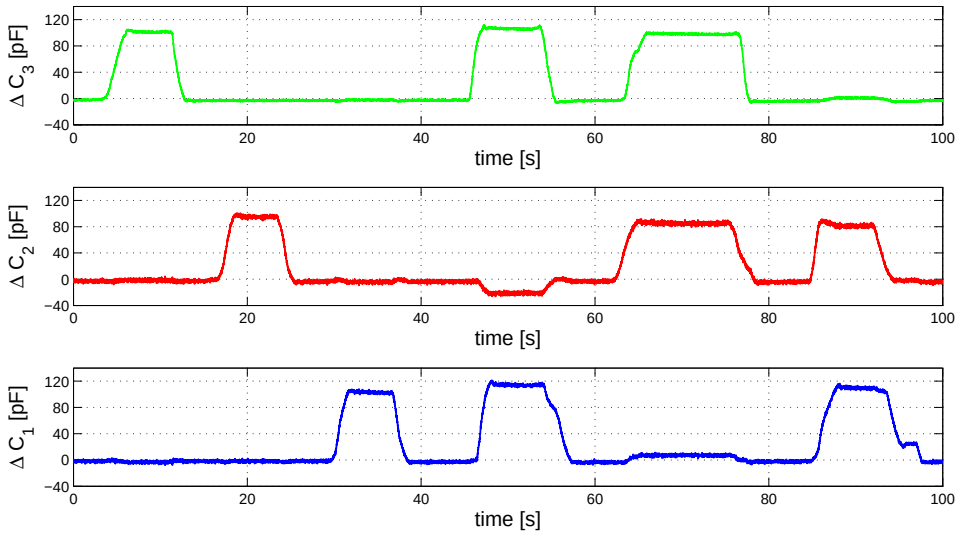

Figure 12. Capacitance changes due to individual and simultaneous stretch

In the second half of the plot, the sensors were stretched simultaneously. As intended, the distributed sensing method delivered a separate reading for each sensor. However, the crosstalk caused by simultaneous stretching was more pronounced than in the previous experiment, because the coefficients a_{ij} were determined for individually stretched sensors. Nevertheless, the results demonstrated the feasibility of measuring three separate capacitance changes through only one sensing channel, and two wires.

6. CONCLUSION

Utilising a transmission line assembled from conductive fabric sensors and external resistors, a distributed sensing method for large scale body motion capture was developed and investigated experimentally. The transmission line was connected to the sensing electronics with only one channel, and two wires. Transmission line capacitance was measured by applying excitation signals with different frequencies. A linear relationship between capacitance changes occurring at each frequency was assumed. This assumption allowed a linear system of equations to be established, which consisted of the variables ΔC_1, ΔC_2 and ΔC_3, and measured coefficients and parameters. The solution of this system of equations was implemented in LabVIEW. On this basis, individual capacitance change readings for each sensor were delivered, even when sensors were stretched simultaneously. In contrast to the presented prototype, a conventional sensing method would have required three sensing channels and six wires, to achieve the same task.

The fairly simplistic linear model, however, has the disadvantage of causing crosstalk between measurements of the stretched sensor, and those of the stationary sensors. This is most likely caused by the assumption of the coefficients a_{ij} being constant over all elongations. Furthermore, the coefficients were only determined with each sensor stretched individually. As can be seen in Fig. 12, this led to more pronounced crosstalk in cases where sensors were stretched simultaneously. In wearable motion capture, however, other non-ideal effects are potentially more significant, such as slippage between skin, garments and attached sensors. In comparison, crosstalk might not be as relevant as it appears to be in this laboratory based experiment. Machine learning algorithms for gesture recognition are trained to recognise patterns in sensor signals, and can therefore handle crosstalk very well, as long as it occurs in the pattern repeatedly.

Future improvements of the distributed sensing method will include the development of a more sophisticated nonlinear mathematical model. Eliminating the linearisation is expected to reduce crosstalk notably. The improved model should also deliver absolute sensor capacitances, rather than capacitance changes. The current model requires the coefficients to be redefined experimentally, whenever the prestrain is changed, and therefore the resting position is shifted. Once the distributed sensing method is refined in these aspects, an investigation into the maximum number of sensors on one set of wires will follow.

ACKNOWLEDGMENTS

We thank StretchSense Ltd for Andreas Tairych's PhD funding support and for providing production facilities and materials for the fabrication of the sensors used in this study.

REFERENCES

[1] H.-K. Lee, S.-I. Chang, and E. Yoon, "A flexible polymer tactile sensor: Fabrication and modular expandability for large area deployment," *Journal of microelectromechanical systems* **15**(6), pp. 1681–1686, 2006.

[2] M.-Y. Cheng, B.-T. Liao, X.-H. Huang, and Y.-J. Yang, "A flexible tactile sensing array based on novel capacitance mechanism," in *Solid-State Sensors, Actuators and Microsystems Conference, 2009. TRANSDUCERS 2009. International*, pp. 2182–2185, IEEE, 2009.

[3] S.-J. Woo, J.-H. Kong, D.-G. Kim, and J.-M. Kim, "A thin all-elastomeric capacitive pressure sensor array based on micro-contact printed elastic conductors," *Journal of Materials Chemistry C* **2**(22), pp. 4415–4422, 2014.

[4] M. Sergio, N. Manaresi, M. Tartagni, R. Guerrieri, and R. Canegallo, "A textile based capacitive pressure sensor," in *Sensors, 2002. Proceedings of IEEE*, **2**, pp. 1625–1630, IEEE, 2002.

[5] J. Meyer, B. Arnrich, J. Schumm, and G. Troster, "Design and modeling of a textile pressure sensor for sitting posture classification," *IEEE Sensors Journal* **10**(8), pp. 1391–1398, 2010.

[6] J. K. Abraham, S. Sullivan, and S. Ranganathan, "Low-cost and disposable pressure sensor mat for non-invasive sleep and movement monitoring applications," in *Engineering in Medicine and Biology Society, EMBC, 2011 Annual International Conference of the IEEE*, pp. 4745–4748, IEEE, 2011.

[7] D. Xu, A. Tairych, and I. A. Anderson, "Localised strain sensing of dielectric elastomers in a stretchable soft-touch musical keyboard," in *SPIE Smart Structures and Materials+ Nondestructive Evaluation and Health Monitoring*, pp. 943025–943025, International Society for Optics and Photonics, 2015.

[8] D. Xu, A. Tairych, and I. A. Anderson, "Stretch not flex: programmable rubber keyboard," *Smart Materials and Structures* **25**(1), p. 015012, 2015.

[9] D. Xu, A. Tairych, and I. A. Anderson, "Where the rubber meets the hand: unlocking the sensing potential of dielectric elastomers," *Journal of Polymer Science Part B: Polymer Physics* **54**(4), pp. 465–472, 2016.